This article has been accepted for publication in a future issue of this journal, but has not been fully edited. Content may change prior to final publication. Citation information: DOI 10.1109/TMECH.2018.2801787, IEEE/ASME Transactions on Mechatronics

MR Safe Robotic Manipulator for MRI-guided Intra-cardiac Catheterization

Kit-Hang Lee*[1], Denny K.C. Fu*[1], Ziyan Guo[1], Ziyang Dong[1], Martin C.W. Leong[1], Chim-Lee Cheung[1], Alex P.W. Lee[2], Wayne Luk[3], *Fellow, IEEE*, Ka-Wai Kwok[1]

***Abstract*—This article introduces a robotic manipulator to realize robot-assisted intra-cardiac catheterization in magnetic resonance imaging (MRI) environment. MRI can offer high-resolution images to visualize soft tissue features such as scars or edema. We hypothesize that robotic catheterization, combined with the enhanced monitoring of lesions creation using MRI intra-operatively, will significantly improve the procedural safety, accuracy and effectiveness. This is designed particularly for cardiac electrophysiological (EP) intervention, which is an effective treatment of arrhythmia. We present the first MR Safe robot for intra-cardiac EP intervention. The robot actuation features small hysteresis, effective force transmission and quick response, which has been experimentally verified for its capability to precisely tele-manipulate a standard clinically used EP catheter. We also present timely techniques for real-time positional tracking in MRI and intra-operative image registration, which can be integrated with the presented manipulator to improve the performance of tele-operated robotic catheterization.**

***Index Terms*— MR Safe robot, robot-assisted intervention, MR image registration, positional tracking in MRI.**

I. Introduction

Catheterization involves dexterous manipulation of thin and flexible medical-grade instruments to pinpoint target anatomy for biopsy, drug delivery or lesion ablation through the transluminal, intraluminal, intracavitary or intracranial surgical approach. Such surgical manipulation could be applied to cardiovascular intervention, prostate surgery, stereotactic neurosurgery or breast biopsy. Cardiovascular diseases, which remain the major cause of mortality in developed countries, particularly demand dexterous catheterization. Heart rhythm disorder (known as arrhythmia) is a typical example, to which cardiovascular electrophysiology (EP) is known as an effective surgical treatment [1, 2]. In the procedure, electrophysiologists insert a long catheter mostly from the femoral vein to the heart chamber, in which radiofrequency (RF) ablation is performed at the catheter tip in contact with lesion tissue to isolate the abnormal electrophysiological signals that cause arrhythmias.

Even with catheter navigation using a cardiac EP roadmap, manipulating the catheter to the desired location remains challenging due to the inconsistent control of a thin (Ø<3mm), long (≈1.5m), flexible EP catheter within rapidly deforming cardiovascular tissue, such as the left ventricle (LV) and left atrium (LA). This challenge has drawn attention to the development of tele-operated robotic platforms, including well-known commercial platforms such as Hansen Sensei® X, and Amigo Remote Catheter System. These platforms aim to improve the dexterity and accuracy of catheter manipulation for intra-cardiac EP intervention.

Apart from dexterous maneuvering of cardiac catheters to the target tissues, both for electro-anatomical (EA) mapping (EP's diagnostic phase) and then RF ablation, the ability to intra-operatively assess lesion locations and their ablation progress is another very crucial factor to enhance the safety and efficacy of the EP procedure. Magnetic resonance imaging (MRI) is a unique image modality capable of offering excellent image contrast for cardiovascular soft tissues, forming a 3D cardiac roadmap online. Additionally, MRI-guided EP avoids exposing patients and clinicians to harmful radiation as generated by X-ray and computed tomography (CT) in conventional EP procedures. Late gadolinium enhancement T2-weighted cardiac MRI [3] can also readily visualize the physiological change of tissues, and identify the scars or edema arising from successful or incomplete RF ablation. Many research groups (e.g. [4-7]) have already conducted numerous patient trials and demonstrated the significant clinical value with the use of intra-operative (intra-op) MRI for EP in clinical routines.

Despite the significant benefits of robot-assisted catheterization as well as the advances of intra-op MRI, no existing commercial robotic catheterization platform is MR-compatible. The main contribution of this work is the development of an MR Safe robotic manipulator (**Fig. 1**) for intra-cardiac catheterization. Detailed design features and its hydraulic actuation mechanism are described (**Section II**), together with experimental evaluations (**Section III**) for tele-manipulation of a clinically used catheter. We also review some state-of-the-art enabling techniques for MRI-guided intervention assisted by tele-operated robots (**Section IV**). Demonstration of the basic robot components and the integrated control interface for MRI guided EP are also

[1]K.H. Lee, D.K.C. Fu, Z. Guo, Z. Dong, M.C.W. Leong, C.L. Cheung, and K.W. Kwok are with Department of Mechanical Engineering, The University of Hong Kong, Hong Kong (e-mail: kwokkw@hku.hk).

[2]A.P.W. Lee, is with Prince of Wales Hospital, The Chinese University of Hong Kong, Hong Kong.

[3]W. Luk, is with Department of Computing, Imperial College London, UK.

* indicates the joint first authorships

This work is supported in part by the Croucher Foundation, the Research Grants Council (RGC) of Hong Kong (17202317, 17227616 and 27209515), the UK Engineering and Physical Sciences Research Council (EP/P010040/1, EP/N031768/1, EP/L016796/1, EP/L00058X/1), the European Union Horizon 2020 Research and Innovation Programme (671653), Aptorum Group Limited and Signate Life Sciences Limited.

This article has been accepted for publication in a future issue of this journal, but has not been fully edited. Content may change prior to final publication. Citation information: DOI 10.1109/TMECH.2018.2801787, IEEE/ASME Transactions on Mechatronics

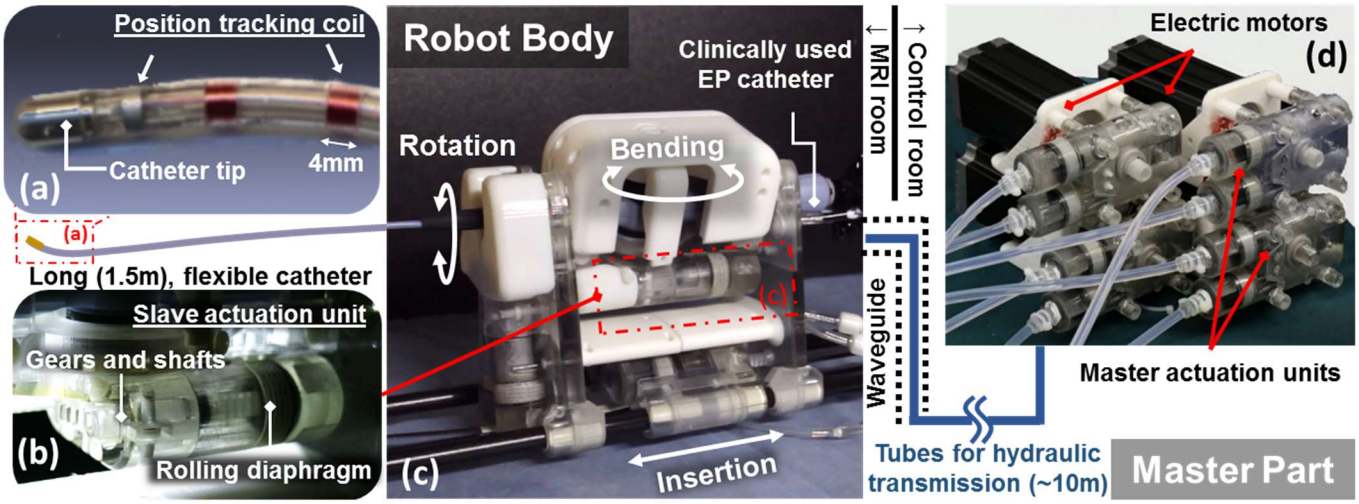

Fig. 1. Overview of the MR Safe hydraulic catheter robotic manipulator showing the allocation of master-slave actuation in MRI room setting; **(a)** Two small active tracking coils wired along the catheter for real-time positional MR-tracking of its tip; **(b)** The MR Safe robotic platform plugged-in with a standard EP catheter for RF ablation. The master-slave actuation units provide rotation, bending, coarse and fine insertion of the catheter; **(c)** Bending actuation unit that transmits the linear hydraulic actuation of rolling diaphragm into rotary motion. All hydraulic actuation units and the robot body are made of MR Safe materials; **(d)** Master electric motor units located in the control room serving as the source of hydraulics. The hydraulic fluid is transmitted to the slave catheter robot platform in MRI room via long (≈10m) hydraulics pipelines. These hydraulics tubes can be channeled through the waveguide.

highlighted in the attached video.

II. Design of MR Safe Robotic Components

Fig. 1 illustrates the key components of the proposed MR Safe robotic manipulator. Such system has to comply with four major design requirements for clinical application: **R1)** the robot operation must not pose any hazard to the patient and to the MRI scanner, and does not adversely affect the quality of MR images; **R2)** the robot has to be compatible with clinically-used catheter and the corresponding 3D cardiovascular navigation system; **R3)** the robot can enable precise actuation with sufficient degrees of freedom (DoFs) to carry out intra-cardiac catheterization, comparable to manual control of the catheter; **R4)** the robot should be compact, light-weight and easy to sterilize. The key robotics components to fulfill these requirements are proposed in the following sections.

A. Master-slave hydraulic actuation units

In MRI environments, electromagnetic (EM) and electrically conductive components have to be handled with caution. Any electric current would inevitably induce EM interference that disrupts the magnetic or gradient field homogeneity in MRI scanner, deteriorating the image quality. This poses a significant challenge to adopting EM motors in actuation mechanism design, particularly for precise catheterization. A common approach is to isolate the motors with complex EM-shielding within the MRI room. However, it is still technically difficult to filter out high-frequency control signals without affecting motor operation and design compactness. Recently, an advanced design on piezoelectric motor has been shown to reduce signal-to-noise ratio (SNR) loss to less than 15% using high-frequency signal transmission [8]. To this end, we aim at developing intrinsically MR Safe and fluid-driven actuators, so that no EM material/power will exist in the MRI room. Previous examples are the MR Safe pneumatic stepper motor presented in [9, 10] and the MR Safe pneumatic needle-guide robot [11].

To address R1, master-slave hydraulic transmission is adopted in the design of actuation units (**Fig. 2**) to drive a catheter. In contrast to pneumatic actuation, hydraulic actuation uses incompressible fluid as working media, offering more steady transmission and quicker response. In the proposed robot, each master unit is actuated by an electric DC motor located in the control room. Each slave unit operates on the patient table near the MRI scanner. Such separation ensures negligible EM interference to the MR images, and allows the compact design of the slave units. During operation, each master unit drives the corresponding slave unit and

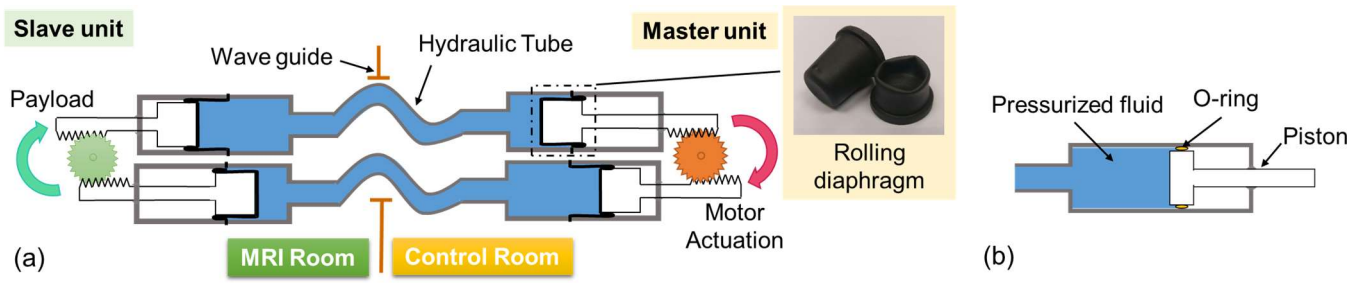

Fig. 2. **(a)** Conceptual design of master-slave hydraulic transmission to ensure MR-compatibility of robot actuation. The contact between the gear teeth can be maintained by preloading fluid pressure, thus minimizing backlash. Rolling diaphragms are adopted to tightly sealed the pressurized fluid. **(b)** Conventional sealing using O-rings may induce significant sliding friction inside the cylinders.

This article has been accepted for publication in a future issue of this journal, but has not been fully edited. Content may change prior to final publication. Citation information: DOI 10.1109/TMECH.2018.2801787, IEEE/ASME Transactions on Mechatronics

subsequently the catheter, via two long pipelines (≈10m each) through the waveguide in-between the control room and the MRI room.

To achieve efficient transmission, rolling diaphragms [12] are employed to seal every master and slave actuation units (**Fig. 2**). Compared to the sealing approaches using O-ring, rolling diaphragms can offer effective sliding with negligible friction between the piston and the inner wall of the cylinder, thus reducing energy loss during actuation. This kind of elastomeric sealing is made of MR Safe, non-metallic material reinforced by fabric to withstand the high internal fluid pressure.

The slave actuation would be lagged behind the master input, for example, caused by the backlash between gears or long hydraulic transmission via flexible pipelines. This lagged phenomenon is known as hysteresis that may significantly affect the performance of the catheter robot. The gear backlash can be reduced by loading higher pressure inside the pipelines such that the pressurized fluid always pushes the pistons toward the gears, thereby keeping the teeth in contact (**Fig. 2**). The effects of preloading pressure on the robot's dynamic performance are experimentally analyzed in section III.

B. Catheter robot design and structure

To address R3, the robot employs *four* pairs of the master-slave actuation units (**Fig. 3**), providing steering, rotation, coarse and fine translation of the catheter with sufficient motion ranges (**Table 1**). The coarse and fine translation DoFs enable, respectively, the longer journey navigation from vessels to the heart chambers, and the shorter range of dexterous tip movement inside the heart chambers for EA mapping and delicate RF ablation. Because the stroke lengths of the rolling diaphragms are limited, the ranges of motion at the rotation and the coarse translation DoFs are magnified using gearboxes at the corresponding slave units. The coarse translation DoF is belt-driven and shares the same moving axis with the fine translation DoF. The steering angle of the catheter tip depends on the choice of the catheter. For example, the Thermocool® SmarttouchTM Bi-Directional Catheter (Biosense Webster Inc.) can be steered up to 180° in two directions.

TABLE I – SPECIFICATIONS OF THE MR SAFE MANIPULATOR

Size	780×105×210 mm^3
Weight	3.16kg (The whole slave body)
Hydraulic pipelines	Length: ≈10 m; Outer/Inner diameter: 6/4mm (Nylon: DG-5431101, Daoguan Inc,)
Transmission media	Pressurized (≤ 0.3 MPa) distill water
Rolling diaphragms	Diameter: 18mm; Stroke length 35mm (MCS2018M, FEFA Inc.)
Power source	Four DC motors with 500 pulses encoder (Maximum torque 278mNm; Gear ratio 14:1, HFmotor-40150, Chengdu Hangfa Hydraulic Engineering Co., Ltd)
Range of motion:	(Equivalent motion to encoder resolution)
Steering	$-45° \le \theta_s \le 45°$ (0.063°)
Rotation	$-360° \le \theta_r \le 360°$ (0.504°)
Coarse translation	$0\text{mm} \le d_c \le 200\text{mm}$ (0.115mm)
Fine translation	$0\text{mm} \le d_f \le 30\text{mm}$ (0.016mm)

To address R2, the angular positions of the master gears can be precisely controlled (**Table 1**) using the motors' built-in proportional–integral–derivative (PID) controllers. Since pipeline diameter and length also contribute to the fluid dynamics [13], stiff pipelines made of nylon (**Table I**) are employed to minimize the pipe deformation when subjected to transmission force, thereby maintaining high precision output at the slave gears.

The modularized catheter holders (**Fig. 3a**) can be tailor-made for various kinds of steerable EP catheters (e.g. Biosense Webster Inc. or St. Jude Medical). It allows switching between different catheterization system simply by replacing the detachable catheter holders. A "plugging-in" mechanism is also designed to facilitate fast and reliable replacements. These catheter holders can be 3D-printed to account for future upgrades of any new catheter handle design.

To minimize the EM interference to the MR images, all the components of the slave system are made of MR Safe materials. Nonconducting, nonmetallic and nonmagnetic items may be

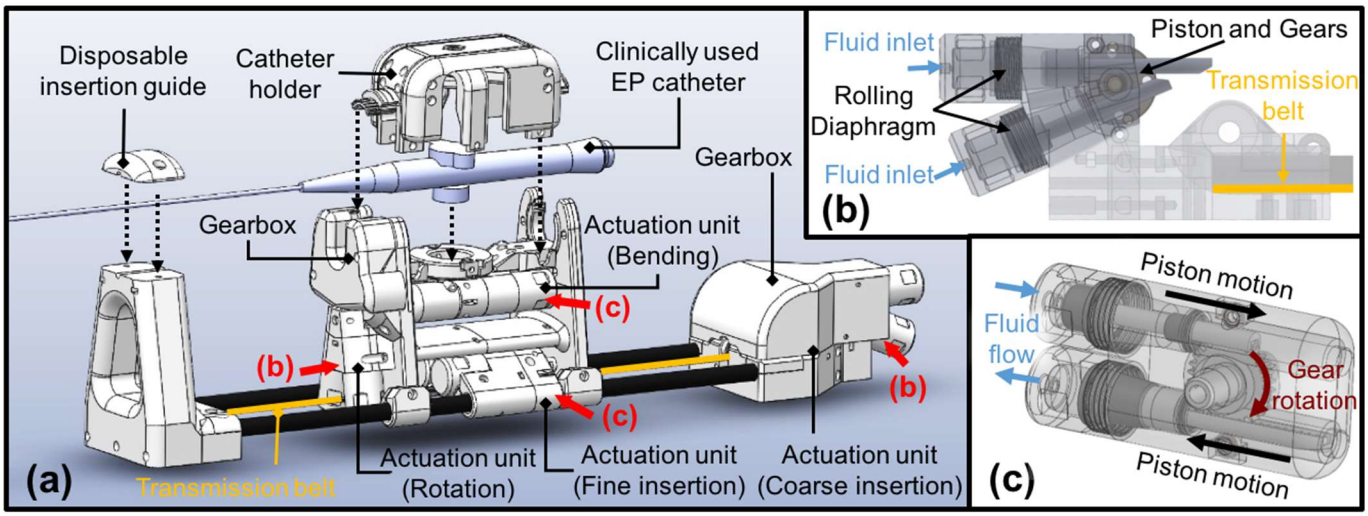

Fig. 3 (a) Main components of the MR Safe robotic manipulator (the slave system) which operates in the MRI room. A clinically used EP catheter can be tightly mounted on a tailor-made catheter holder. (b) and (c): The actuation units providing steering, rotation, coarse and fine translation of the catheter.

This article has been accepted for publication in a future issue of this journal, but has not been fully edited. Content may change prior to final publication. Citation information: DOI 10.1109/TMECH.2018.2801787, IEEE/ASME Transactions on Mechatronics

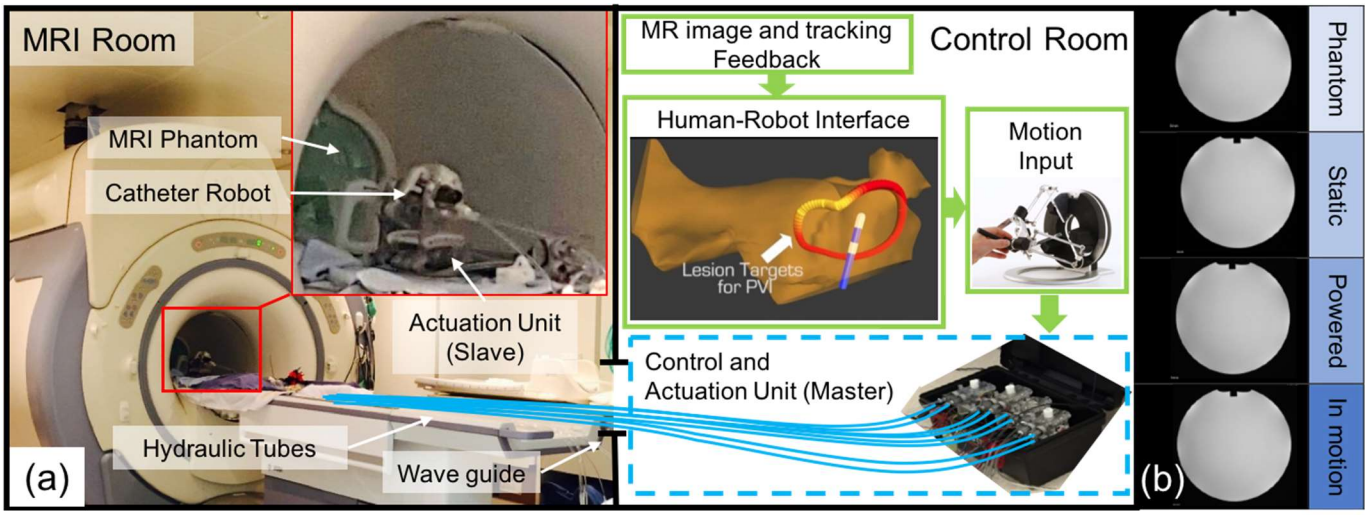

Fig. 4. (a) Experimental setup of MR-compatibility test for the presented robot. Key components are connected between the MRI and the control rooms via the wave guide. The operator can tele-manipulate the catheter using the catheter navigation interface. (b) MR images of an MRI phantom placed aside the robot indicate the negligible EM interference in four different operating conditions.

determined to be MR Safe by providing scientifically based rationale rather than test data [14]. The main structural components are 3D-printed using acrylic compounds (VeroWhitePlus/VeroClear, Stratasys, USA). The key actuation components include gears made of nylon, a transmission belt made of rubber, and auxiliary parts made of polymers (e.g. Polyvinyl Chloride (PVC), Polyetherimide (PET)). This master-slave system has been tested to withstand rapid actuation ($\leq$ 15Hz) under high fluid pressure ($\leq$ 0.3MPa). To address R4 regarding sterilization, this small-sized slave body can be enclosed by disposable surgical equipment drapes. The insertion guide (**Fig. 3**) made of low-cost acrylic compounds, is also disposable and can be sterilized beforehand.

III. Experimental Performance Evaluation

To validate the robot performance for MRI-guided robot-assisted catheterization, we have conducted: **A)** An MRI-compatibility test; **B)** performance analyses of the master-slave hydraulic actuators; and **C)** A lab-based simulated ablation task on a left atrium (LA) phantom model.

A. MR-compatibility test

The slave robotic manipulator placed in MRI room complies with the MR Safe classification of American Society for Testing and Materials (ASTM) standard F2503-13 [14], in which the robot comprises solely nonconducting, nonmetallic and nonmagnetic materials. For the safety concerns of experiment, some components were double-confirmed using metal/magnetic detectors before their integration. We simulated the basic operation for testing the compatibility with the MRI (**Fig. 4a**). The master system was actuated inside the control room inside a 1.5T MRI scanner (SIGNA, General Electric Company, USA). The slave system was placed adjacent to a standard MRI phantom (J8931, J.M. Specialty Parts, USA) filled with distilled water. The phantom was placed at the iso-center of the scanner, and then imaged to evaluate the potential EM interference generated by the slave robotic manipulator.

Fig. 4b depicts the resulting MR images of the phantom under four different conditions: **i)** *Phantom*: only the phantom alone was placed in the scanner; **ii)** *Static*: the robot introduced and remained power OFF; **iii)** *Powered*: the robot was kept still, but with the hydraulic and electric power ON in the control room; and **iv)** *In motion*: the robot was in operation, manipulating the EP catheter. Condition **(i)** serves as the baseline for evaluation. The EM-induced effects on the MR images were measured based on the changes in the signal-to-noise ratio (SNR) $J = I/\sigma$, where I is the mean intensity value of a 40×40 pixels region at the image center, and σ is the standard deviation of intensity value in a region of 40×40 pixels at the lower right corner [15]. The MR images had maximum SNR loss less than 2% and had no observable image artifacts during the robot operation.

B. Hydraulic transmission performance

In the proposed master-slave actuators, the hydraulic transmission fluid was pre-pressurized in order to diminish the hysteresis due to gear backlash or the long (≈10m) hydraulic transmission (**section II-A**). However, the excessive preload pressure also led to severe gear and pivot friction, which may in turn degrade the manipulation precision. In this section, we first evaluated the force transmission performance, and then analyzed the position tracking accuracy and the effects of preload fluid pressure on the hysteresis, as well as on the resultant dynamic performance.

1) Force Transmission

The force transmission performance of the master-slave actuator is evaluated with a free weight-lifting experiment. In this experiment, a rotary slave actuator depicted in **Fig. 1c** is coupled to a winch of 5cm radius. With the hydraulic fluid pre-loaded at 0.1MPa, the master-slave actuator is capable of lifting 3kg at a constant velocity of 10.01 cm/s, corresponding to an output torque of 1.47 Nm and net power of 2.93 W. The input torque at the motor axis on master side is also monitored by a torque sensor, which is used to estimate the hydraulic force transmission efficiency as 70%. Such force transmission

This article has been accepted for publication in a future issue of this journal, but has not been fully edited. Content may change prior to final publication. Citation information: DOI 10.1109/TMECH.2018.2801787, IEEE/ASME Transactions on Mechatronics

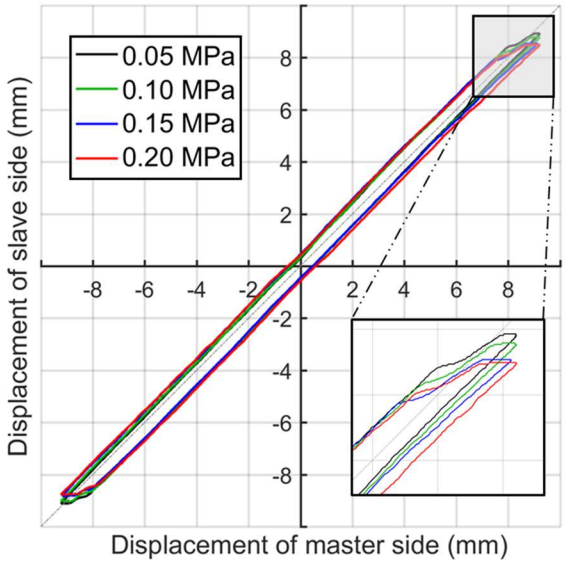

Fig. 5. Hysteresis of the master-slave actuation unit at different preload fluid pressure. The average values of hysteresis were 0.88mm, 0.93mm, 1.02mm, 1.29mm for preloaded pressure 0.05 MPa, 0.1 MPa, 0.15 MPa and 0.2 MPa, respectively.

performance is more than sufficient to steer the rotor on the standard catheter handle in full range, to roll the catheter (>360°), and also to push/pull the catheter (<230mm) through the introducer sheath and the guiding tube.

In fact, the maximum torque of the present prototype is limited by the mechanical strength of the 3D printed components. In the real practice for human trials, the robot prototype ought to be fabricated with standard industrial machining procedures. Wider choices of MR Safe materials, such as Acetal (POM) or Nylon or any strong resilient plastic, will be used to comprise more robust structure for promising durability and enhanced actuation torque.

2) Hysteresis

Hysteresis is the primary concern for intra-cardiac intervention that requires accurate manipulation of the catheter with high resolution. The hysteresis of the pair of master-slave actuation units was measured and shown in **Fig. 5**. The translational positions of the master and slave pistons were measured at different levels of preloaded fluid pressure inside the pipelines. The periodic motion of the master unit was controlled by the embedded PID positional controller at a frequency of 0.1Hz, where 70% of the stroke-length was covered. **Fig. 6** depicts that the slave actuation unit could precisely follow a sinusoidal trajectory of the master unit, with a maximum absolute error of 0.67mm. The hysteresis was largely uniform throughout the whole range of motion, particularly at higher preloaded pressure. The hysteresis only slightly increase with the preloaded pressure, potentially due to the rise in static friction between the gears.

3) Dynamic response

The dynamic performance of the master-slave actuation units for different values of preloaded fluid pressure was investigated using a frequency response method. Given a sinusoidal torque input $\tau = A\sin(\omega t)$ to the master gear, where ω was the frequency and t was the time, the torque at the slave gear was measured. The amplitude A was set to 0.1

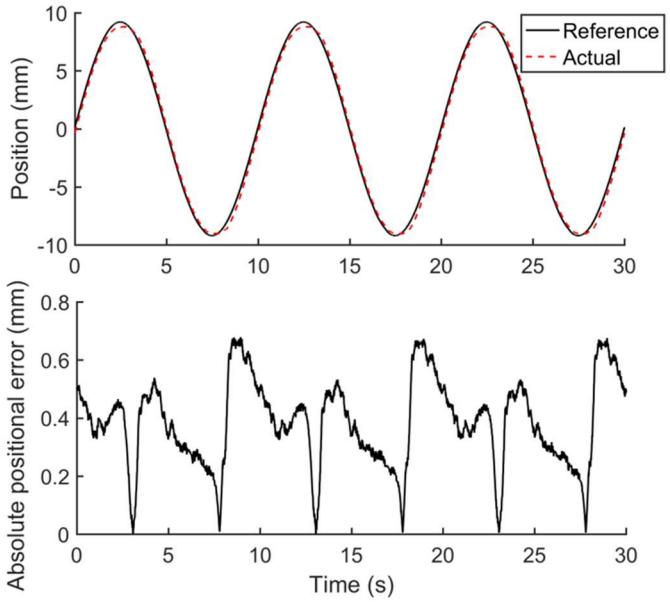

Fig. 6. Periodic motion of the master-slave actuation unit pre-loaded with 0.1 MPa of fluid pressure. The slave position (dash line, upper plot) could precisely follow the sinusoidal reference trajectory (concrete line, upper plot) of the master unit at 0.1 Hz. The absolute error (lower plot) has a maximum of 0.67 mm.

Nm, which is within the nominative operation range of the motor. **Fig. 7** depicts the Bode plot that characterizes the "magnification" M and the "phase-shift" ξ of the hydraulic transmission at steady state. Note that for a linear time invariant system, the frequency response at steady state becomes $\tau_{ss} = MA\sin(\omega t + \xi)$.

The magnitude plot indicates that the magnification increases with the preloaded fluid pressure. The magnification value peaks at around 5 Hz, which corresponds to the natural frequencies of the overall hydraulic transmission. We also found that the increase of the preloaded fluid pressure does not significantly affect the natural frequency.

The phase lag of the transmission was kept at around 25˚ for low actuation frequency (≤ 1 Hz), and was not significantly

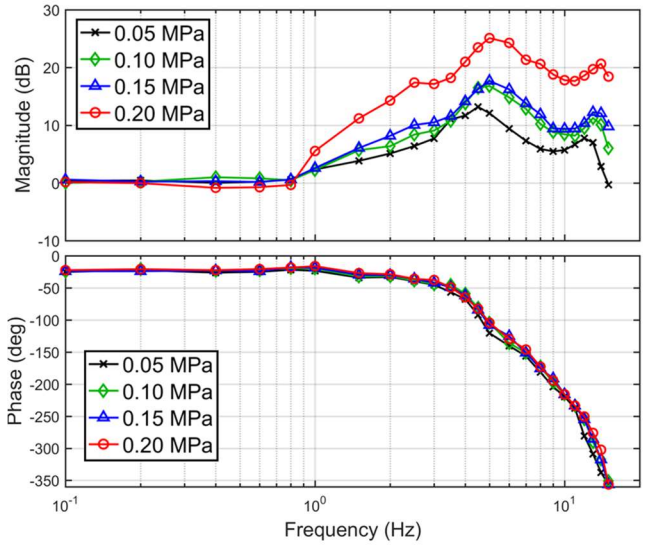

Fig. 7. Bode plot showing torque transmission response of the master-slave hydraulic actuation unit at four different levels of preloaded fluid pressure. The magnitude (top) and phase shift (bottom) are shown. The data were collected from 10 cycles at the steady state.

This article has been accepted for publication in a future issue of this journal, but has not been fully edited. Content may change prior to final publication. Citation information: DOI 10.1109/TMECH.2018.2801787, IEEE/ASME Transactions on Mechatronics

affected by the variation of the preloaded fluid pressure. The transmission had small time delay: 45ms and 66ms at actuation frequency 1 Hz and 15 Hz, respectively, with preloaded fluid pressure 0.2 MPa. Such phase-shift and the natural frequency could result from the compliance of the 10m long nylon tubes, rolling diaphragms. However, the actual transmission performance also depends on the complicated fluid dynamics, it will require further investigations based on dynamic modelling techniques to explain for the frequency response.

In summary, the master-slave actuator had small (1.29 mm at 0.1 Hz) hysteresis and quick response (66 ms at 15 Hz), even at a high preloaded fluid pressure (0.2 MPa). Although the increase of the preloaded fluid pressure slightly increased the hysteresis (from 0.88 mm at 0.05 MPa to 1.29 mm at 0.2 MPa), it could attain effective force transmission as shown in the Bode plot (**Fig. 7**). As a result, it demonstrates that acceptable system delay could be maintained in a normative operating frequency the for catheterization. Apart from the preloaded fluid pressure, fluid properties such as mass and viscosity would also affect the transmission. We employed distilled water as hydraulic fluid due to its ease of implementation and availability. The hydraulic pipelines length and diameter are also part of design considerations in regard to actuation dynamics. Previous analytical studies and experimental investigations [13] have suggested that the fluid friction can be reduced by using pipelines with a larger diameter, resulting in better system efficiency and smaller transmission phase lag; In addition, shorter pipelines are also preferable, which could reduce the transmission fluid inertia and also increase the transmission stiffness.

C. Catheter manipulation for pulmonary vein isolation

The robotic catheterization performance was validated by a simulated task of pulmonary vein isolation (PVI), which is a treatment of atrial fibrillation. PVI requires RF ablation conducted inside the left atrium (LA). A typical task is to make lesion scars along the ostia of the left superior and inferior pulmonary veins. Such consistent scars would isolate the abnormal electrical signal originated from the arrhythmias, which causes the irregular heart motion [16].

In our lab-based validation, a standard EP ablation catheter (Thermocool® SmarttouchTM Bi-Directional Catheter, Biosense Webster Inc.) was "plugged-in" to the slave robot.

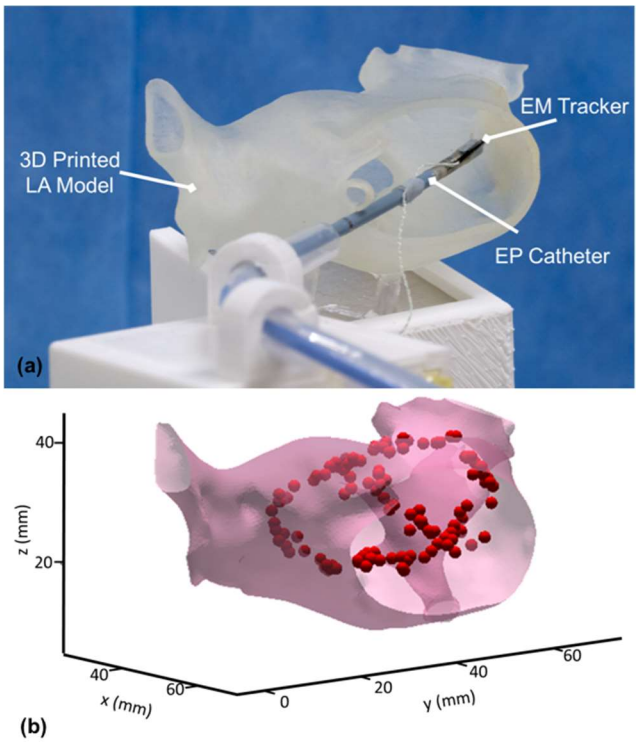

Fig. 8. (a) Experiment settings of the PVI task. A catheter was tele-manipulated by the proposed robot to perform "ablation" on the left atrium (LA) phantom model. (b) Locations of the ablations (127 points) on the interior surface.

An EM positional sensor (NDI Medical Aurora) was attached close to the catheter tip in order to track the 3-D tip positions in real-time. The phantom LA was a 3D-printed model made of soft material (AgilusClear, Stratasys Inc.) according to real anatomical data. In this task, the subject could tele-manipulate the catheter mounted the robot using a motion input device (Novint Falcon, NF1-L01-004). He/she was advised to press the foot pedal, then activate the "RF ablation", once being able to confirm the proper tip contact with the lesion targets prescribed on the virtual LA model. Note that the 3-D tracking coordinates, along with the virtual model, have to be well aligned with the actual LA phantom (**Fig. 8a**).

A reachability test was conducted with the aim to verify if the catheter tip driven by the presented robot is capable to reach or cover the region of interest along the ostia of the left superior and inferior pulmonary veins. **Fig. 8b** depicts the measured footprint of the catheter tip along the ostia, which are the

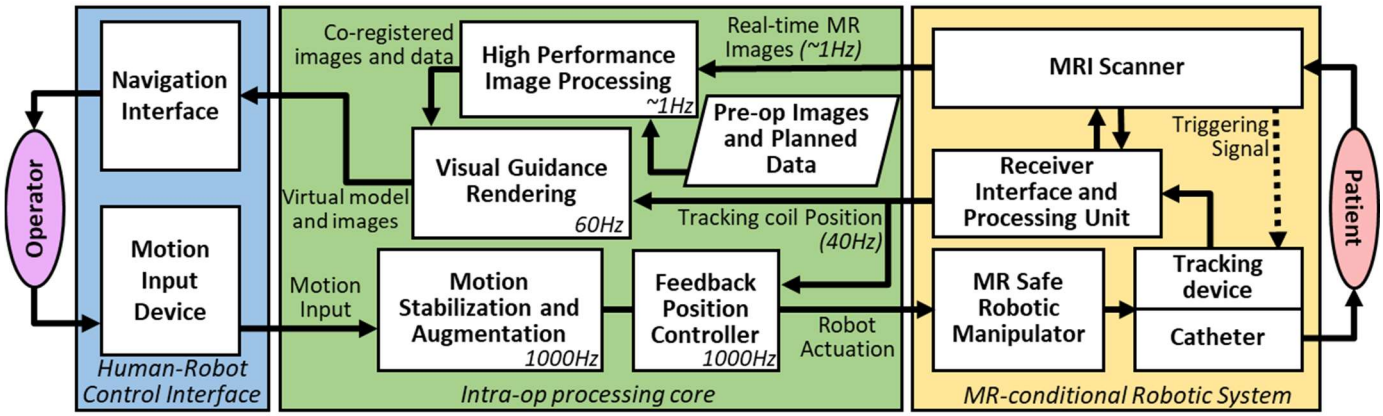

Fig. 9. Schematic diagram of the MRI-guided robot-assisted catheterization. The operator can perform robotic EP catheterization in a closed-loop manner.

This article has been accepted for publication in a future issue of this journal, but has not been fully edited. Content may change prior to final publication. Citation information: DOI 10.1109/TMECH.2018.2801787, IEEE/ASME Transactions on Mechatronics

ablation points confirmed by the operator during the tele-manipulation. Note that the robot catheterization precision should be taken into account, only if having detailed kinematic/dynamic study of the catheter itself. Such a study currently lies beyond the scope of this paper. In the real MRI-guided EP, such real-time 3-D tracking of the catheter can be achieved by MRI, also in the same image coordinate frame. Further details are discussed in Section IV.

IV. Towards MRI-guided and Robot-assisted Catheterization

Apart from the robot hardware, accurate MR-based localization of the catheter, as well as high-performance image registration, are of importance to realizing intra-op MRI-guided EP catheterization. In this section, MR-tracking and intra-operative image registration techniques are reviewed. We also discuss the prospective integration of these two components into a human-robot control interface, which will enable a closed-loop control of the proposed robot under MRI. **Fig. 9** illustrates this closed-loop architecture.

A. Real-time Positional Tracking in MRI

Tracking the catheter position is essential in many cardiac interventions. This positional feedback data will close the control loop of robotic navigation (**Fig. 9**). MR-based tracking can be achieved by attaching two tiny solenoid coils (**Fig. 1**) close to the catheter tip, which are connected to a receiver electronic system via coaxial cables. This is a typical MR-*active* tracking setting, in which the coil can actively "pick up" the MR gradient field [17] along the three principal directions for localization. By matching/tuning the receiver's LC components for a specific MRI scanner, these coils can be highly sensitive to very local field inhomogeneity [18] without adversely affecting the image quality, providing high resolution ($0.6\times0.6\times0.6\text{mm}^3$) tracking performance with fast sampling rate (40 Hz) [19].

In contrast, the conventional use of *passive* MR fiducial markers is found to be difficult in achieving responsive/ continuous tracking. Complicated MRI sequence is required, taking significant time to process susceptibility artefacts in the high-resolution images for fast and accurate localization. Recently, paramagnetic markers can be automatically localized at high frequency (50 Hz), but with a relatively large positional error of ≤ 4.5mm when the MRI sequence PRIDE was used to acquire echo-phased projection in three principal axes [20].

MR-*semi-active* tracking is a state-of-the-art approach, in which coils are integrated into small isolated LC circuits. These coils resonate with specific MR frequencies by means of wireless inductive coupling with the MRI system. There are no direct capacitive electrical connections with the MRI system. This avoids resonating RF waves along the coaxial cables connection, which can pose potential heating hazard in active tracking (**Table II**). Using a properly programmed MR sequence that detunes/triggers the isolated resonant circuit, the semi-active device can be visualized in the MR images. To alter the RF resonant behaviour, an optical fibre could be connected to the circuit in order to illuminate a photodiode placed parallel to a coil, which could achieve real-time imaging (20fps) in an *in vivo* test [21].

MR-tracking also allows real-time visualization of the catheter configuration with respect to the EP roadmap constructed from the MR images. This could provide the operator with reliable navigation guidance and consistent motion reference to aim the catheter tip at the ablation lesions imaged and registered locally around the tip (**Fig. 4**). Such intra-operative visualization will involve fast image registration, which is described in the next section. A demonstration can be found in the attached video.

B. Intra-operative MR Image Registration

With zero EM interference accredited to the proposed MR Safe hydraulic actuators, fast MR images can be acquired in the region around the catheter tip being tracked. Thus, the post-ablation lesions (edema or scars) can be promptly visualized and selected on T2-weighted MR images. These physiological changes need to be instantly overlaid on the EP roadmap, allowing the electrophysiologist to determine whether the ablation is applied sufficiently to the lesions. However, such intra-op MR images are mostly obtained at different cardiac cycles from the pre-operative (pre-op) images that construct the EP roadmap. Non-rigid image registration is the prerequisite to continuously re-align the selected lesion on the EP roadmap (**Fig. 10**).

Intensity-based registration methods are usually employed,

TABLE II – Technologies Reviewed for Positional Tracking in MRI

	Operating principles	Advantages	Disadvantages
Passive Tracking	- Encapsulated -ve/+ve contrast agents causing MR signal void or T1 shortening. - Encapsulated materials visible by non-proton multispectral	- Simple and safe integration - Capable of operating under different field strengths	- Time consuming - Tracking cannot be switched on/off
Active Tracking	- Use image sequence to induce position-dependent MR gradient field within a volume of interest - Detect the MR gradient field using micro coil/antenna in frequency domain	- High spatial and temporal resolution of 3-D tracking information - Easy to conduct automatic tracking and slice plane following	- Potential risk of RF heating on wires connected to receiver - Sophisticated tuning/matching the circuity in the receiver interface required
Semi-active Tracking	- Isolated LC circuit with photodiode/photoresistor connected in parallel is designed to resonate at MRI Larmor frequency	- No electric wire connected with the scanner receiver - Optically-controllable resonance behavior	- Difficulty in assembly and miniaturization - Sophisticated design of tracking sequence needed

This article has been accepted for publication in a future issue of this journal, but has not been fully edited. Content may change prior to final publication. Citation information: DOI 10.1109/TMECH.2018.2801787, IEEE/ASME Transactions on Mechatronics

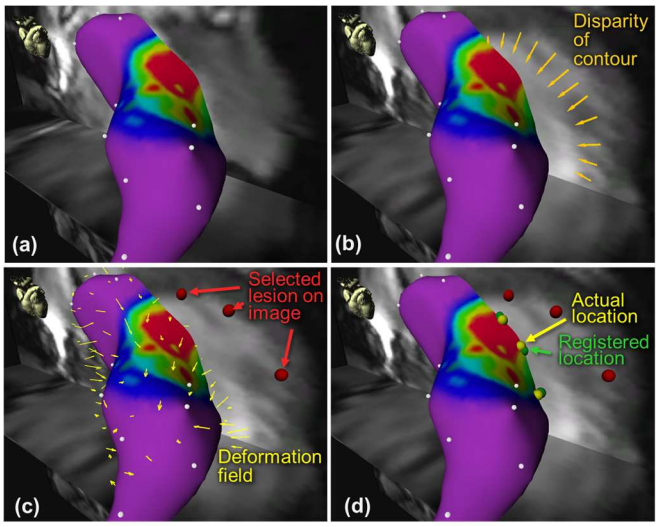

Fig. 10. **(a)** 3-D EP roadmap of left ventricle segmented and rendered based on pre-op MR images; **(b)** Significant disparity (indicated by orange arrows) between the roadmap and intra-op images during the diastole; **(c)** Ablation landmarks selected on a slice of 2D intra-op MR images. Yellow flow arrows are shown as the deformation field estimated by the *Demons*-based registration method; **(d)** The landmarks re-aligned appropriately on the 3D roadmap based on the deformation field.

given the advantage of its higher tolerance of MR image noise and artefact, compared to the feature-based methods. *Diffeomorphic demons* [22] is a typical intensity-based approach, however, the computation is usually intensive. For example, our computer system currently takes 2 minutes and 30 seconds to process two sets of MR images with size of 256×256×181 pixels. However, prolonged computation time required to align the target lesions frequently with the roadmap will undoubtedly hinder the surgical workflow. We have proposed that this computation bottleneck can be resolved using high-performance computing architectures [23, 24], such as graphical processing units (GPUs). GPUs facilitate spatial parallelism by simultaneously sharing the computation load with thousands of its processing units under the "Single Instruction, Multiple Data (SIMD)" architecture. Vectorized data types (e.g. float4) by cascading multiple primitive data (e.g. 32-bit float) also allow full utilization of the memory bus in GPU, as well as batch processing of multiple data under a single instruction.

Reconfigurable computing technology, such as field-programmable gate arrays (FPGAs), can also be employed to accelerate image registration and related applications. FPGAs' flexible architecture can effectively exploit temporal parallelism by customizing stream processing pipelines [25]. Furthermore, the bit-width of the data streams in FPGAs can be optimized based on trade-offs between computation speed and accuracy. As a result, co-registration between two sets of 3D images (192×132×300 pixels) could be achieved within 1.1 seconds [24]. Such rapid realignment of the intra-op image is crucial to achieving precise catheter manipulation in dynamic surgical scenarios. This fast MR registration would offer effective visual guidance in the human-robot control interface (**Fig. 4**) that will be incorporated into our proposed robotic manipulator. Other robot motion planning tasks such as proximity query can also be accelerated by FPGAs [26].

C. *Human-Robot Control Interface*

Intra-op imaging can be applied in conjunction with MR-tracking, such that the tracking is interleaved with the MR image sequence. This tracking involves measurement of both 3D position and orientation of the catheter tip. These data can be continuously streamed to the EP navigation system and the robot control interface [27]. Note that the entire MR-based catheter tracking takes place in the same MR imaging coordinate system. Unlike conventional EP, our MR-based approach does not require external tracking reference, thereby avoiding potential disparity caused by relative registrations between tracking and imaging system. This enables rendering of the virtual endoscopic view from the viewpoint of the catheter tip [28]. Such virtual view facilitates fine placement of the catheter tip while approaching ablation targets registered on the roadmap (**Fig. 4**). Moreover, robotic control methods that account for the catheter's kinematics/dynamics [29] could also be applied to provide the operator with a consistent manipulation reference upon this 2D endoscopic view, as demonstrated in our attached video.

V. Conclusion

The proposed MR Safe robotic manipulator is the first of its kind that offers sufficient DoFs to tele-manipulate a cardiac catheter under intra-op MRI guidance [30]. The robot fulfils the MR Safe standard (ASTM F2503-13), as it solely comprises of nonconductive, nonmetallic and nonmagnetic materials. Currently, there is no such commercial system that is MR compatible/conditional.

The proposed highly-efficient hydraulic transmission using rolling-diaphragm has been shown to have great potential for offering high-performance actuation under MRI without adversely affecting imaging quality (SNR loss <2%). This master-slave actuation system involves an advanced sealing method which has demonstrated its advantages in low-friction, quick-response and low-noise motion transmission. The slave actuation unit can output torque up to 1.47Nm with a force transmission efficiency of 70%. Such actuation torque can be transmitted from the control room into the MRI room via 10m long hydraulics pipelines that are channeled through the waveguide, while maintaining a small overall mechanical backlash of 0.88mm by applying appropriate hydraulic pressure at 0.05 MPa. The incompressibility of hydraulic fluid also results in stable and low-latency dynamic response (<70ms), even at high-frequency motion (15Hz). The proposed manipulator is capable of performing a simulated pulmonary vein isolation procedure, demonstrating its sufficient workspace and dexterity for EP catheterization.

Our ongoing work is to improve hydraulic actuation to offer a full range of catheter advancement along the vessels to the chamber. Furthermore, MR-tracking and intra-operative image registration techniques are also essential to realize MRI-guided EP catheterization. Advanced MR-tracking devices can be used to localize the catheter tip at high frequency (40Hz) and resolution ($0.6\times0.6\times0.6mm^3$) in the image coordinates, thus enabling accurate alignment of catheter configuration with the

roadmap. Fast image registration implemented on advanced GPU/FPGA-based architecture can rapidly register/realign (~1.1s) the lesions on the pre-op EP roadmap. The RF ablation progress can then be frequently monitored by the intra-op MR images. It avoids manual coordination of such lesions on the MR images which may not be consistent with the roadmap at different points of the cardiac cycle.

In summary, the advent of the proposed MRI-guided catheter robotic system will increase confidence to perform RF ablation completely, while improving the safety of catheter navigation. As a result, it may reduce nerve damage, esophageal fistula creation, pulmonary vein stenosis and stroke, as well as the chance of post-procedural disease recurrence (currently 30% in atrial fibrillation (AF) and 50% in ventricular tachycardia). This will contribute to justifying the use of MRI, while reducing the overall healthcare expenditure of the treatments.

REFERENCES

[1] F. Morady, "Radio-frequency ablation as treatment for cardiac arrhythmias," *New England Journal of Medicine,* vol. 340, no. 7, pp. 534-544, 1999.

[2] M. Haïssaguerre *et al.*, "Spontaneous Initiation of Atrial Fibrillation by Ectopic Beats Originating in the Pulmonary Veins," *New England Journal of Medicine,* vol. 339, no. 10, pp. 659-666, 1998.

[3] E. J. Schmidt *et al.*, "Electro–Anatomic Mapping and Radio–Frequency Ablation of Porcine Left Atria and Atrio-Ventricular Nodes using Magnetic Resonance Catheter Tracking," *Circulation: Arrhythmia and Electrophysiology,* p. CIRCEP. 109.882472, 2009.

[4] R. Razavi *et al.*, "Cardiac catheterisation guided by MRI in children and adults with congenital heart disease," *The Lancet,* vol. 362, no. 9399, pp. 1877-1882, 2003.

[5] R. C. Susil, C. J. Yeung, H. R. Halperin, A. C. Lardo, and E. Atalar, "Multifunctional interventional devices for MRI: a combined electrophysiology/MRI catheter," *Magnetic resonance in medicine,* vol. 47, no. 3, pp. 594-600, 2002.

[6] S. R. Dukkipati *et al.*, "Electroanatomic mapping of the left ventricle in a porcine model of chronic myocardial infarction with magnetic resonance–based catheter tracking," *Circulation,* vol. 118, no. 8, pp. 853-862, 2008.

[7] A. N. Raval *et al.*, "Real-time MRI guided atrial septal puncture and balloon septostomy in swine," *Catheterization and cardiovascular interventions,* vol. 67, no. 4, pp. 637-643, 2006.

[8] H. Su *et al.*, "Piezoelectrically actuated robotic system for MRI-guided prostate percutaneous therapy," *IEEE/ASME Transactions on Mechatronics,* vol. 20, no. 4, pp. 1920-1932, 2015.

[9] D. Stoianovici, A. Patriciu, D. Petrisor, D. Mazilu, and L. Kavoussi, "A new type of motor: pneumatic step motor," *IEEE/ASME Transactions On Mechatronics,* vol. 12, no. 1, pp. 98-106, 2007.

[10] Y. Chen, K.-W. Kwok, and Z. T. H. Tse, "An MR-Conditional High-Torque Pneumatic Stepper Motor for MRI-Guided and Robot-Assisted Intervention," *Annals of Biomedical Engineering,* journal article vol. 42, no. 9, pp. 1823-1833, 2014.

[11] D. Stoianovici *et al.*, "Multi-Imager Compatible, MR Safe, Remote Center of Motion Needle-Guide Robot," *IEEE Transactions on Biomedical Engineering,* 2017.

[12] J. P. Whitney, M. F. Glisson, E. L. Brockmeyer, and J. K. Hodgins, "A low-friction passive fluid transmission and fluid-tendon soft actuator," in *IEEE/RSJ International Conference on Intelligent Robots and Systems*, 2014, pp. 2801-2808: IEEE.

[13] G. Ganesh, R. Gassert, E. Burdet, and H. Bleuler, "Dynamics and control of an MRI compatible master-slave system with hydrostatic transmission," in *IEEE International Conference on Robotics and Automation* 2004, vol. 2, pp. 1288-1294: IEEE.

[14] *ASTM F2503-13, Standard Practice for Marking Medical Devices and Other Items for Safety in the Magnetic Resonance Environment, ASTM International, West Conshohocken, PA*, 2013, www.astm.org.

[15] K. Chinzei, R. Kikinis, and F. A. Jolesz, "MR compatibility of mechatronic devices: design criteria," in *International Conference on Medical Image Computing and Computer-Assisted Intervention*, 1999, pp. 1020-1030: Springer.

[16] H. Oral *et al.*, "Catheter ablation for paroxysmal atrial fibrillation," *Circulation,* vol. 108, no. 19, pp. 2355-2360, 2003.

[17] J. L. Duerk, E. Y. Wong, and J. S. Lewin, "A brief review of hardware for catheter tracking in magnetic resonance imaging," *Magnetic Resonance Materials in Physics, Biology and Medicine,* vol. 13, no. 3, p. 199, 2002.

[18] A. Glowinski, G. Adam, A. Bücker, J. Neuerburg, J. J. van Vaals, and R. W. Günther, "Catheter visualization using locally induced, actively controlled field inhomogeneities," *Magnetic resonance in medicine,* vol. 38, no. 2, pp. 253-258, 1997.

[19] W. Wang *et al.*, "Real-time active MR-tracking of metallic stylets in MR-guided radiation therapy," *Magnetic resonance in medicine,* vol. 73, no. 5, pp. 1803-1811, 2015.

[20] S. Patil, O. Bieri, P. Jhooti, and K. Scheffler, "Automatic slice positioning (ASP) for passive real-time tracking of interventional devices using projection-reconstruction imaging with echo-dephasing (PRIDE)," *Magnetic resonance in medicine,* vol. 62, no. 4, pp. 935-942, 2009.

[21] S. Weiss *et al.*, "In vivo safe catheter visualization and slice tracking using an optically detunable resonant marker," *Magnetic resonance in medicine,* vol. 52, no. 4, pp. 860-868, 2004.

[22] T. Vercauteren, X. Pennec, A. Perchant, and N. Ayache, "Diffeomorphic demons: Efficient non-parametric image registration," *NeuroImage,* vol. 45, no. 1, pp. S61-S72, 2009.

[23] K. W. Kwok *et al.*, "Interfacing fast multi-phase cardiac image registration with MRI-based catheter tracking for MRI-guided electrophysiological ablative procedures," *Circulation,* vol. 130, no. Suppl 2, pp. A18568-A18568, 2014.

[24] K. W. Kwok *et al.*, "FPGA-based acceleration of MRI registration: an enabling technique for improving MRI-guided cardiac therapy," *Journal of Cardiovascular Magnetic Resonance,* vol. 16, no. S1, p. W11, 2014.

[25] W. Atabany and P. Degenaar, "A Spatiotemporal Parallel Image Processing on FPGA for Augmented Vision System," in *Advances in Computer and Information Sciences and Engineering*: Springer, 2008, pp. 558-561.

[26] T. C. Chau *et al.*, "Acceleration of real-time Proximity Query for dynamic active constraints," in *Field-Programmable Technology (FPT), 2013 International Conference on*, 2013, pp. 206-213: IEEE.

[27] Y. Feng *et al.*, "An efficient cardiac mapping strategy for radiofrequency catheter ablation with active learning," *International Journal of Computer Assisted Radiology and Surgery,* vol. 12, no. 7, pp. 1199-1207, July 01 2017.

[28] Y. Chen *et al.*, "Augmented Reality for Improving Catheterization in Magnetic Resonance Imaging-Guided Cardiac Electrophysiology Therapy1," *Journal of Medical Devices,* vol. 8, no. 2, pp. 020917-020917-2, 2014.

[29] C. L. Cheung *et al.*, "Kinematic-model-free positional control for robot-assisted cardiac catheterization," in *Proceedings of The Hamlyn Symposium on Medical Robotics*, 2016, p. 80.

[30] Z. Guo, Z. Dong, K.-H. Lee, D. K. Fu, and K.-W. Kwok, "Robotic Catheter System for MRI-guided Cardiovascular Interventions," Patent US15/630,406; PCT/CN2017/089701, 2016.